Inorganic Chemistry

pubs.acs.org/IC

Article

Spectroscopic and Theoretical Investigation of Color Tuning in Deep-Red Luminescent Iridium(III) Complexes

Thomas M. Stonelake, Kaitlin A. Phillips, Haleema Y. Otaif, Zachary C. Edwardson, Peter N. Horton, Simon J. Coles, Joseph M. Beames,* and Simon J. A. Pope*

Cite This: *Inorg. Chem.* 2020, 59, 2266−2277

Read Online

ACCESS | Metrics & More | Article Recommendations | Supporting Information

ABSTRACT: A series of heteroleptic, neutral iridium(III) complexes of the form $[Ir(L)_2(N^O)]$ (where L = cyclometalated 2,3-disubstituted quinoxaline and N^O = ancillary picolinate or pyrazinoate) are described in terms of their synthesis and spectroscopic properties, with supporting computational analyses providing additional insight into the electronic properties. The 10 $[Ir(L)_2(N^O)]$ complexes were characterized using a range of analytical techniques (including ^1H, ^{13}C, and ^{19}F NMR and IR spectroscopies and mass spectrometry). One of the examples was structurally characterized using X-ray diffraction. The redox properties were determined using cyclic voltammetry, and the electronic properties were investigated using UV−vis, time-resolved luminescence, and transient absorption spectroscopies. The complexes are phosphorescent in the red region of the visible spectrum (λ_{em} = 633−680 nm), with lifetimes typically of hundreds of nanoseconds and quantum yields ca. 5% in aerated chloroform. A combination of spectroscopic and computational analyses suggests that the long-wavelength absorption and emission properties of these complexes are strongly characterized by a combination of spin-forbidden metal-to-ligand charge-transfer and quinoxaline-centered transitions. The emission wavelength in these complexes can thus be controlled in two ways: first, substitution of the cyclometalating quinoxaline ligand can perturb both the highest occupied molecular orbital (HOMO) and lowest unoccupied molecular orbital levels (LUMO, Cl atoms on the ligand induce the largest bathochromic shift), and second, the choice of the ancillary ligand can influence the HOMO energy (pyrazinoate stabilizes the HOMO, inducing hypsochromic shifts).

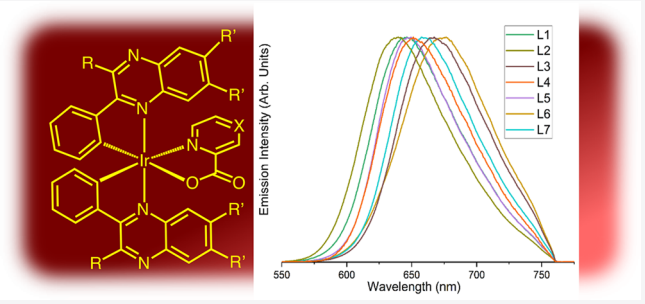

INTRODUCTION

The development and study of luminescent cyclometalated iridium(III) complexes continue to attract significant attention.[1] The motivation is driven by the use of such species in optoelectronic applications such as bioimaging,[2] electroluminescence,[3] photoredox catalysis,[4] nonlinear optics,[5] chemosensing,[6] and energy upconversion.[7] Underpinning these applications is the ability to control the physical properties of the complex and, in particular, tuning[8] of the electronic properties that dictate the emission characteristics. This can be achieved by the careful consideration and combination of conjugated cyclometalated ligands and the choice of the ancillary ligand.[9] In this context, the vast majority of Ir(III) complexes employ five-membered chelate ligands (for example, 2-phenylpyridine), which result in either neutral or cationic[10] species. A handful of reports have also detailed six-membered chelate systems, which can also have attractive luminescence properties.[11]

The development of red-emissive Ir(III) complexes is very attractive from a number of perspectives. First, interest in red emitters has been driven by the advance of white-light-emitting diodes, which require high-purity blue-, green-, and red-emitting materials.[12] The advantage of Ir(III) coordination chemistry is that ligands can be developed to tune emission across the visible-light spectrum, although the purity of the emission colors can be compromised by the spectral broadness of the emission bands. For this application, the development of Ir(III) red phosphors is challenging because of the inherently lower quantum efficiencies that result from a lower energy gap between the ground and excited states. Red emitters are also very attractive in bioimaging disciplines using confocal fluorescence microscopy;[13] the use of longer excitation and emission wavelengths tends to be more compatible with biological samples, can significantly improve imaging quality through reduced autofluorescence signals, and is complementary to the plethora of commercially available dyes.

A general strategy for bathochromically shifting the emission wavelengths of Ir(III) complexes is to increase conjugation of

Received: October 10, 2019
Published: February 4, 2020

https://dx.doi.org/10.1021/acs.inorgchem.9b02991
Inorg. Chem. 2020, 59, 2266−2277

Scheme 1. General Molecular Structure of the Complexes under Investigation

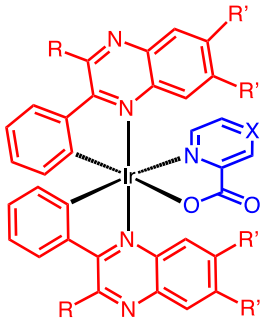

[R = Me, Ph; R' = Me, Cl, F; X = C, N]

the chelating ligands and introduce substituents for further tuning. For example, exchanging 2-phenylpyridine for 1-phenylisoquinoline (i.e., comparing $[Ir(ppy)_3]$ vs $[Ir(piq)_3]$) results in a red shift in the emission for the latter to around 620 nm.[14] Researchers have further developed this strategy,[15] including the use of various ancillary ligands.[16] Indeed, a number of reports have also shown that emission wavelengths can be shifted further into the near-IR (>750 nm) region, although quantum efficiencies are correspondingly lower.[17] Our own contributions have focused upon the development of substituted 2-phenylquinoline[18] and 2-phenylquinoxaline[19] as cyclometalating ligands. Quinoxalines, in particular, provide an adaptable ligand platform for developing red-emitting Ir(III) complexes with good photostability.[20]

Herein, we report the development of a series of neutral, mixed-ligand Ir(III) complexes (Scheme 1), where emission wavelengths can be tuned 633 nm < λ < 680 nm by simple variations in the cyclometalating quinoxaline ligand structure and the choice of the ancillary ligand.[21] A combination of detailed spectroscopic and computational analyses have been used to unravel the origins of the luminescence behavior and fully ascribe the excited-state properties, providing a working hypothesis for the rational design of complexes based on these ligands.

RESULTS AND DISCUSSION

Synthesis of the Complexes. The tetrasubstituted quinoxaline-based ligands (L1−L7), synthesized by the simple condensation of an appropriate aryl diketone with a disubstituted 1,2-phenylenediamine, were reported previously.[7b] From these ligands, a series of chloro-bridged Ir(III) dimeric compounds of the formula $[\{Ir(L)_2(\mu\text{-}Cl)\}_2]$ were synthesized according to the traditional method first published by Nonoyama.[22] First, these dimeric Ir(III) species were then reacted with picolinic acid to yield the corresponding charge-neutral picolinate complexes $[Ir(L)_2(pic)]$ (where L = L1−L7; Figure 1). This approach was also adopted in the isolation of selected pyrazinoate variants (Figure 2), $[Ir(L)_2(pyz)]$ (where L = L2, L5, and L7), with the exception of $[Ir(L2)_2(pyz)]$, where improved yields were obtained via the bis(acetonitrile) adduct *cis*-$[Ir(MeCN)_2(L2)_2]BF_4$. Complete experimental and synthetic details, as well as characterization data, are presented in the Supporting Information.

Characterization of the Complexes. The complexes synthesized in this study were characterized by a range of techniques including ^1H, $^{13}C\{^1H\}$, and $^{19}F\{^1H\}$ NMR spectroscopy, in addition to high-resolution mass spectrometry. All of the complexes showed good solubility in common organic solvents such as chloroform, acetonitrile, methanol, and acetone.

Inclusion of the asymmetric picolinate or pyrazinoate ligand in the coordination sphere renders the two cyclometalated quinoxaline ligands inequivalent. This increases the complexity of the resulting NMR spectra of these species. For example, the

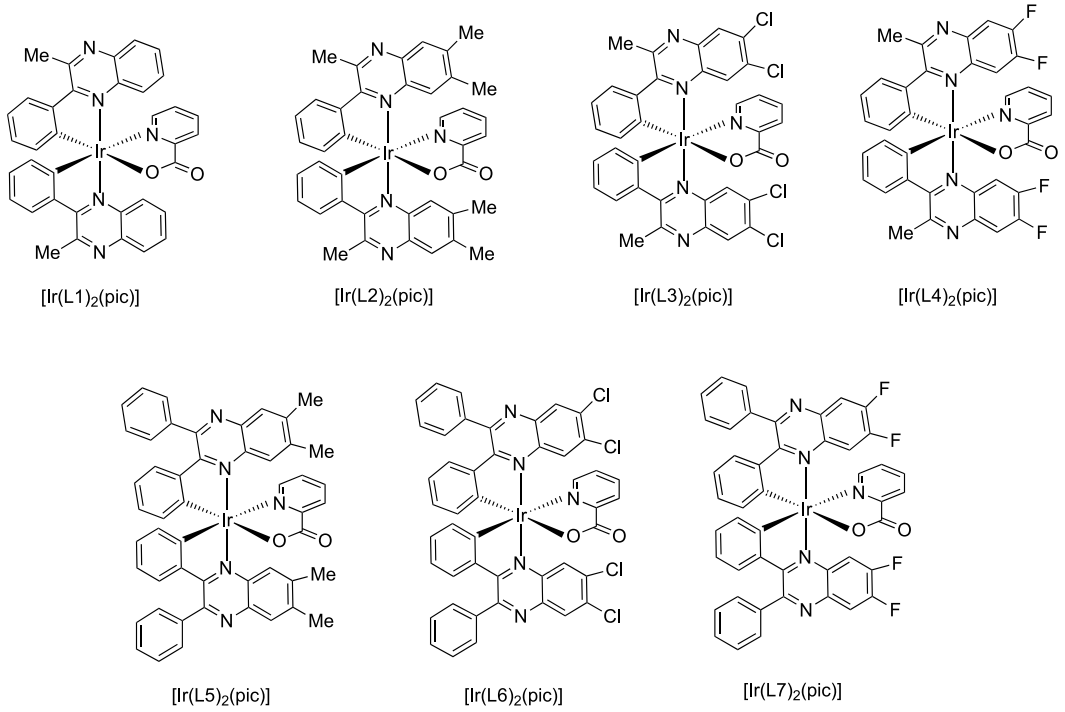

Figure 1. Structures of the mixed-ligand iridium(III) picolinate complexes $[Ir(L)_2(pic)]$.

https://dx.doi.org/10.1021/acs.inorgchem.9b02991
Inorg. Chem. 2020, 59, 2266−2277

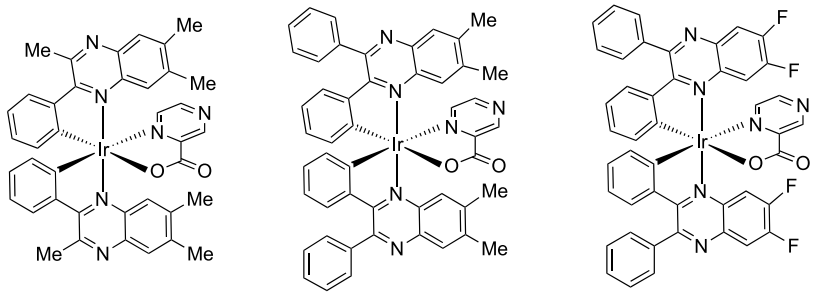

Figure 2. Structures of the mixed-ligand iridium(III) pyrazinoate complexes $[Ir(L)_2(pyz)]$.

Table 1. Comparison of the $^{19}F\{^1H\}$ NMR Data for the Fluorinated Ligands and Complexes

compound	δ_F (ppm)
L4[a]	−130.4 (d, 21 Hz), −131.2 (d, 21 Hz)
L7[a]	−129.9
$[Ir(L4)_2(pic)]$[b]	−131.8 (d, 21 Hz), −132.9 (d, 21 Hz), −133.7 (d, 19 Hz), −134.0 (d, 19 Hz)
$[Ir(L7)_2(pic)]$[b]	−130.2 (d, 19 Hz), −131.5 (d, 19 Hz), −133.1 (d, 21 Hz), −133.6 (d, 22 Hz)
$[Ir(L7)_2(pyz)]$[a]	−123.5 (d, 22 Hz), −128.1 (d, 22 Hz), −128.5 (d, 22 Hz), −130.5 (d, 22 Hz)

[a] $CDCl_3$. [b] CD_3CN.

Table 2. Selected Bond Lengths (Å) and Bond Angles (deg) from the Crystallographic Data of $[Ir(L7)_2(pic)]$

Bond Lengths (Å)			
Ir1−O41	2.156(4)	Ir1−N41	2.195(4)
Ir1−N1	2.055(4)	Ir1−C1	1.980(6)
Ir1−N21	2.066(4)	Ir1−C21	1.981(6)
Bond Angles (deg)			
O41−Ir1−N41	76.10(15)	C1−Ir1−N21	96.8(2)
N1−Ir1−O41	81.47(15)	C1−Ir1−N41	166.5(2)
N1−Ir1−N21	175.58(16)	C1−Ir1−C21	93.3(2)
N1−Ir1−N41	98.55(16)	C21−Ir1−O41	176.21(16)
N21−Ir1−O41	101.02(15)	C21−Ir1−N1	98.61(19)
N21−Ir1−N41	85.63(16)	C21−Ir1−N21	79.15(19)
C1−Ir1−O41	90.41(18)	C21−Ir1−N41	100.17(19)
C1−Ir1−N1	79.5(2)		

^1H NMR spectrum of $[Ir(L1)_2(pic)]$ showed two unique methyl environments at ca. 3.35 ppm, as well as unique resonances for each of the quinoxaline-based protons. The lack of symmetry in these complexes is apparent in comparison to the spectra for the previously reported $[Ir(L1)_2(bipy)]PF_6$, wherein the cyclometalating ligands are equivalent (Figure S1).[7b] Other general features in the ^1H NMR spectra include two upfield doublets at ca. 6−7 ppm, which correspond to the protons ortho to the cyclometalating C atom on each unique quinoxaline ligand. In the majority of cases, the $^{13}C\{^1H\}$ NMR spectra revealed a furthest downfield resonance of ca. 170 ppm, which was assigned to the carbonyl group of the coordinated picolinate or pyrazinoate ligand. The fluorine-containing complexes were also analyzed via $^{19}F\{^1H\}$ NMR spectroscopy, and the data are presented in Table 1 alongside those of relevant free ligands.

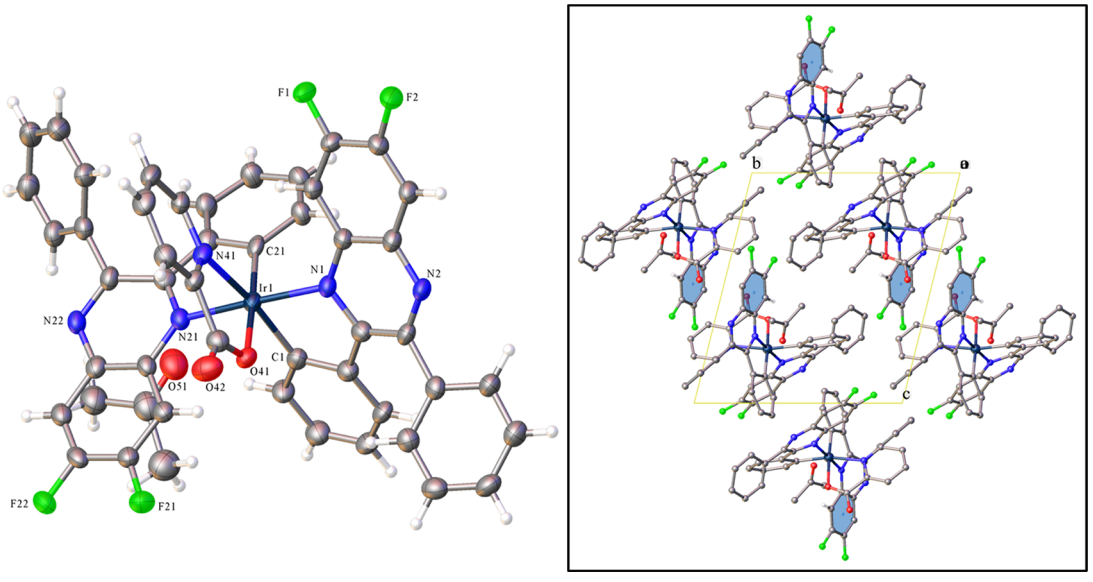

Figure 3. X-ray structure of $[Ir(L7)_2(pic)]$: $C_{49}H_{32}F_4IrN_5O_3$, M_r = 1006.99, triclinic, $P\bar{1}$ (No. 2), a = 11.4642(3) Å, b = 12.2735(2) Å, c = 14.3213(3) Å, α = 76.139(2)°, β = 86.773(2)°, γ = 88.029(2)°, V = 1952.85(7) Å^3, T = 100(2) K, Z = 2, Z' = 1, μ(Cu Kα) = 7.230 mm^{-1}, 51782 reflections measured, 7115 unique (R_{int} = 0.0887), which were used in all calculations. The final wR_2 was 0.1050 (all data), and R_1 was 0.0411 [$I > 2(I)$]. Inset: Packing diagram for $[Ir(L7)_2(pic)]$. Ellipsoids drawn at 50%.

https://dx.doi.org/10.1021/acs.inorgchem.9b02991
Inorg. Chem. 2020, 59, 2266−2277

Table 3. UV−Vis Absorption and Redox Properties of the Complexes

complex	UV−vis absorption[b] λ_{max} (nm)	cyclic voltammetry[a] E_{ox} (V)	E_{red} (V)
$[Ir(L1)_2(pic)]$	274 sh, 364 sh, 373, 491 sh	+1.16	−1.42
$[Ir(L2)_2(pic)]$	276, 381, 507 sh	+1.11	−1.51
$[Ir(L3)_2(pic)]$	273, 300, 371, 389, 538 sh	+1.27	−1.17
$[Ir(L4)_2(pic)]$	272, 361, 377, 501 sh	+1.26	−1.05, −1.27
$[Ir(L5)_2(pic)]$	262, 300, 387, 501 sh	+1.09	−1.25
$[Ir(L6)_2(pic)]$	273, 396, 528 sh	+1.31	−1.12
$[Ir(L7)_2(pic)]$	277, 387, 505 sh	+1.30	−1.24
$[Ir(L2)_2(pyz)]$	267, 380, 480 sh	+1.18	−0.98, −1.35
$[Ir(L5)_2(pyz)]$	271, 386, 489 sh	+1.19	−1.04, −1.42
$[Ir(L7)_2(pyz)]$	272, 383, 494 sh	+1.39	−1.00, −1.15

[a]The oxidation potentials were measured as dichloromethane solutions at 200 mV s^{-1} with 0.1 M $[NBu_4][PF_6]$ as the supporting electrolyte calibrated with Fc/Fc^+ at +0.46 V. [b]Chloroform solutions, 10^{-5} M.

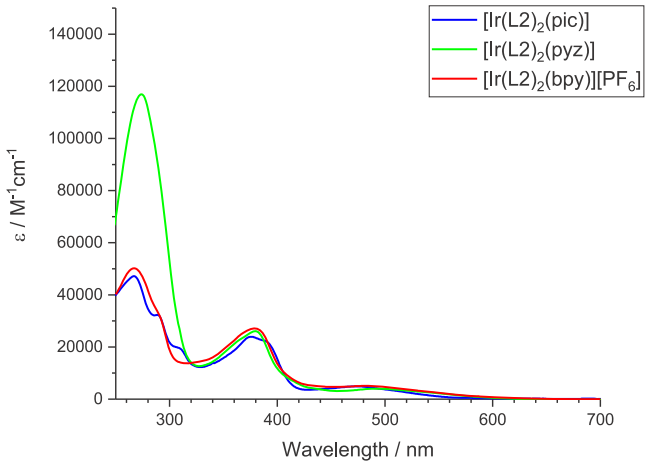

Figure 5. UV−vis absorption spectra showing the influence of the ancillary ligand (picolinate vs pyrazinoate vs bipyridine) across Ir(III) complexes of L2.

Because of the inequivalence of the cyclometalating ligands, four ^{19}F resonances, which appear in the −120 to −140 ppm range, were observed in the $^{19}F\{^1H\}$ NMR spectra for the fluorinated complexes, and thus are consistent with the $[Ir(L)_2(bipy)]PF_6$ analogues. Each resonance appeared as a doublet arising from $^3J_{FF}$ coupling at ca. 19−22 Hz. The ^{19}F resonances of the picolinate species were subtly shifted upfield from the free ligands, whereas for the pyrazinoate species, the resonances were generally downfield. This suggests that the relative donor characteristics of the ancillary ligand can influence the electron density at Ir(III) and thus modulate the electronic environment of the fluorine substituents on the cyclometalated quinoxaline ligands. The $^{19}F\{^1H\}$ NMR data support the notion that picolinate is a stronger donor to Ir(III) than pyrazinoate.

All complexes in this study were also characterized by high-resolution mass spectrometry. In each case, a molecular-ion peak was present and consistent with the expected isotopic distribution for a protonated parent ion, $[M + H]^+$, or a sodium ion adduct, $[M + Na]^+$. In some cases, a fragment was also present that contained both cyclometalating ligands but with a loss of the ancillary ligand (Figure S2).

X-ray Crystallography Structure. Single red plate-shaped crystals of $[Ir(L7)_2(pic)]$ were successfully isolated, from the slow evaporation of an acetone solution of the complex, and then investigated using X-ray diffraction.[23] Data collection parameters are in the caption of Figure 3; see Table 2 for selected bond lengths and bond angles. The structure reveals that the complex crystallized as its acetone solvate, with one molecule of acetone per complex moiety.

The structure confirms the expected coordination sphere at Ir, with the quinoxaline-derived ligands coordinating in a cyclometalating mode, resulting in a cis-C,C and trans-N,N coordination arrangement at Ir(III). The coordinated picolinate ligand is bound to Ir(III) via the N^O chelating mode. The bond lengths within the coordination sphere are closely comparable to those of related complexes that incorporate cyclometalated phenylquinoxaline ligands.[7b] The structure also reveals intermolecular packing supported by $\pi-\pi$ interactions of ca. 3.65 Å (Figure 3, inset) that involve the difluorinated quinoxaline ring.

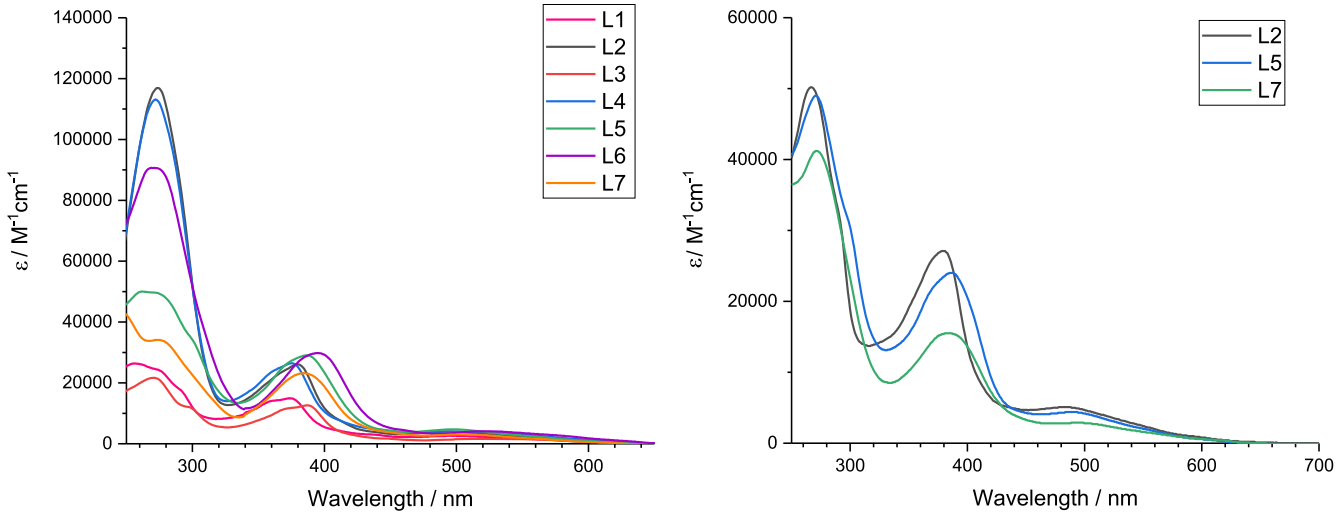

Figure 4. Left: UV−vis absorption spectra recorded for the picolinate complexes. Right: UV−vis absorption spectra recorded for the pyrazinoate complexes. All samples were recorded in chloroform at 10^{-5} M.

https://dx.doi.org/10.1021/acs.inorgchem.9b02991
Inorg. Chem. 2020, 59, 2266−2277

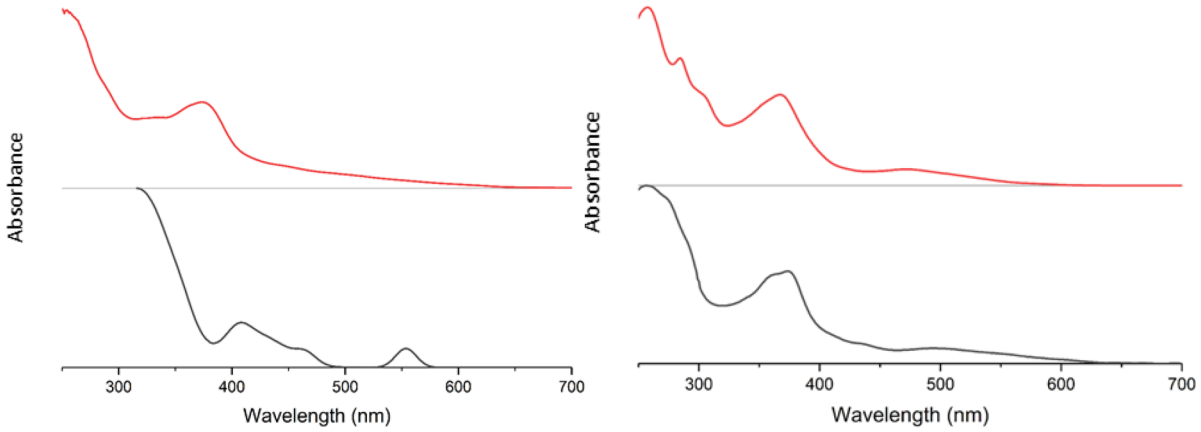

Figure 6. Left: Comparison of the experimental (red) and simulated (black) absorption spectra for $[Ir(L1)_2(pic)]$. In the left-hand panel, the computed spectrum is constructed by convolution of the TD-DFT transition energies and their associated oscillator strengths. The spin-forbidden peak at $\lambda > 500$ nm is shown for reference, with an arbitrary oscillator strength scaled as a guide to the eye. The simulated spectrum is comprised of singlet and triplet transitions from the singlet ground state. Right: Comparison of the observed spectra of $[Ir(L1)_2(pic)]$ (black) and $[Ir(L1)_2(bipy)]PF_6$ (red).

Table 4. Computed Values for the Absorption and Emission Maxima of the Ir(III) Complexes[a]

complex	$S_0 \rightarrow S_1$ (nm)	$S_0 \rightarrow T_1$ (nm)	$T_1 \rightarrow S_0$ (nm)
$[Ir(L1)_2(pic)]$	424	578	697 (6467)
$[Ir(L2)_2(pic)]$	419	568	689 (640)
$[Ir(L3)_2(pic)]$	440	608	739 (665)
$[Ir(L4)_2(pic)]$	428	586	710 (650)
$[Ir(L5)_2(pic)]$	425	579	705 (648)
$[Ir(L6)_2(pic)]$	445	618	751 (680)
$[Ir(L7)_2(pic)]$	434	597	722 (653)
$[Ir(L2)_2(pyz)]$	416	563	685 (633)
$[Ir(L5)_2(pyz)]$	422	573	703 (641)
$[Ir(L7)_2(pyz)]$	431	589	714 (651)

[a]Experimentally determined $T_1 \rightarrow S_0$ values are presented in parentheses.

Electrochemical Properties of the Complexes. The electrochemical characteristics of the Ir(III) complexes were investigated in deoxygenated dichloromethane. Cyclic voltammograms were measured using a platinum disk electrode (scan rate 200 mV s^{-1}; 1×10^{-3} M solutions; 0.1 M $[NBu_4][PF_6]$ as the supporting electrolyte). In most cases, the complexes each showed one oxidative and one reductive process (Table 3). The oxidation process appeared in the range of +1.1 to +1.4 V and was attributed, and found to be generally irreversible, to the $Ir^{3+/4+}$ couple. These oxidative values are lower than those for the corresponding cationic species $[Ir(L)_2(bipy)]PF_6$, which is consistent with an Ir^{3+} center that is more easily oxidized in these neutral species. Within the series of complexes, the substituents of the quinoxaline cyclometalating ligand have a significant influence on the redox potentials: the halogenated complexes have higher oxidation potentials, whereas the methylated variants are most easily oxidized. These observations are again consistent with the relative electron-donating capacity of the coordinated quinoxaline ligands. The ancillary ligand also has a subtle influence on the $Ir^{3+/4+}$ couple, with the pyrazinoate species possessing a more positive oxidation potential than their picolinate counterparts, again consistent with the relative electron-donating capacity of the two ligands. The observed reduction features, most of which were irreversible, are assumed to be ligand-based processes,[7b] with the pyrazinoate complexes introducing a feature around −1 V.

UV−Vis Absorption Properties of the Complexes. The UV−vis absorption spectra of all complexes were recorded as solutions in chloroform at a concentration of 10^{-5} M. Figure 4 shows the spectra recorded for each series. In both sets of spectra, three distinct features can be seen: a peak at around 275−300 nm from ligand-based $\pi-\pi^*$ transitions, a feature at

Table 5. Summary of the Major Calculated Contributions to Each Molecular Orbital from Each Part of the Complex[a]

	Ir 5d		Q1		Q2		pic/pyz
complex	HOMO−1	HOMO	LUMO	LUMO+1	LUMO	LUMO+1	LUMO+2
$[Ir(L1)_2(pic)]$	43	40	36	59	59	36	96
$[Ir(L2)_2(pic)]$	37	39	34	60	60	34	96
$[Ir(L3)_2(pic)]$	41	39	40	55	55	40	94
$[Ir(L4)_2(pic)]$	40	39	39	56	56	39	96
$[Ir(L5)_2(pic)]$	21	38	38	57	57	38	94
$[Ir(L6)_2(pic)]$	21	38	42	53	53	41	6
$[Ir(L7)_2(pic)]$	16	38	41	54	54	41	90
$[Ir(L2)_2(pyz)]$	28	38	48	47	38	39	77
$[Ir(L5)_2(pyz)]$	10	37	41	35	47	48	76
$[Ir(L7)_2(pyz)]$	8	37	44	46	49	46	89

[a]Q1 and Q2 are the inequivalent quinoxaline ligands.

https://dx.doi.org/10.1021/acs.inorgchem.9b02991
Inorg. Chem. 2020, 59, 2266−2277

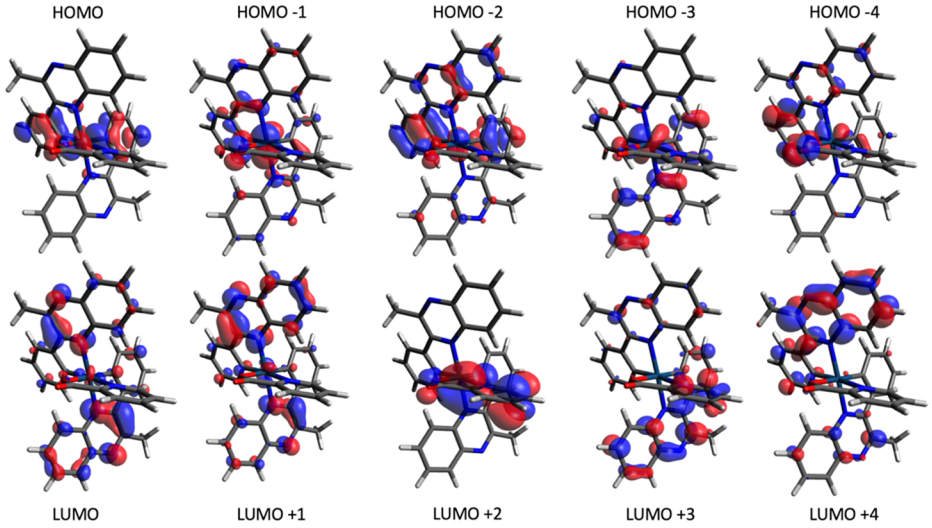

Figure 7. Examples of calculated Kohn–Sham molecular orbitals for $[Ir(L1)_2(pic)]$. Similar representations for all other complexes in the series are available in the Supporting Information.

Table 6. Description of the Calculated Molecular Orbital Contributions, Excited-State Descriptions, and Their Associated Transitions for $[Ir(L1)_2(pic)]$ (pic = Picolinate)[a]

	moiety contributions to the orbital (%)				orbital contributions to the excited states	
orbital	Ir 5d	pic	Q1	Q2	excited state	contributing transitions
LUMO+4	1	1	78	21	1 (423.97 nm; f = 0.0349)	HOMO → LUMO (87%)
LUMO+3	1	23	15	62	2 (415 nm; f = 0.1237)	HOMO → LUMO+1 (84%)
LUMO+2	2	96	2	0		
LUMO+1	4	1	59	36	3 (343.01 nm; f = 0.089)	HOMO−2 → LUMO (37%)
LUMO	4	1	36	59		HOMO−1 → LUMO (43%)
HOMO	40	4	29	27	4 (329.34 nm; f = 0.0442)	HOMO−1 → LUMO+1 (21%)
HOMO−1	43	14	23	20		HOMO−1 → LUMO+1 (48%)
HOMO−2	9	8	51	32	5 (321.19 nm; f = 0.1511)	HOMO−3 → LUMO (38%)
HOMO−3	34	5	14	47		HOMO−2 → LUMO+1 (15%)
HOMO−4	14	19	54	13		

[a]Q1 and Q2 are the different quinoxaline ligands.

Table 7. Calculated Energies of the Frontier Orbitals of the Ir(III) Complexes and Their Differences, Ordered by Decreasing ΔE

complex	HOMO (eV)	LUMO (eV)	ΔE (eV)
$[Ir(L2)_2(pyz)]$	−5.43	−2.41	3.02
$[Ir(L2)_2(pic)]$	−5.33	−2.32	3.01
$[Ir(L5)_2(pyz)]$	−5.44	−2.46	2.98
$[Ir(L1)_2(pic)]$	−5.42	−2.45	2.97
$[Ir(L5)_2(pic)]$	−5.34	−2.38	2.96
$[Ir(L7)_2(pyz)]$	−5.63	−2.73	2.9
$[Ir(L4)_2(pic)]$	−5.53	−2.6	2.93
$[Ir(L7)_2(pic)]$	−5.53	−2.65	2.88
$[Ir(L3)_2(pic)]$	−5.6	−2.75	2.85
$[Ir(L6)_2(pic)]$	−5.61	−2.79	2.82

ca. 375 nm with a shoulder around 430 nm, and a broader feature around 500 nm that tails >600 nm. In the context of previous reports, both ligand-based $\pi-\pi^*$ transitions from the conjugated quinoxalines and spin-allowed metal-to-ligand charge-transfer (MLCT) transitions are likely to contribute to the features at 350–450 nm. Similarly, spin-forbidden transitions, mediated by the heavy Ir atom, to the ^{3}MLCT state are likely to contribute to the weaker feature (typical $\varepsilon \approx 10^3$ M^{-1} cm^{-1}) that dictates the 500–600 nm region of the spectra.

Within the series of picolinate complexes $[Ir(L)_2(pic)]$, variations in the energies of the MLCT features are dictated by the nature of the substituents on the quinoxaline ligands. Similarly, the pyrazinoate complexes $[Ir(L)_2(pyz)]$ show the same principle features in their absorption spectra. A direct comparison between $[Ir(L2)_2(pic)]$ and $[Ir(L2)_2(pyz)]$ shows that the latter possesses subtly, hypsochromically shifted MLCT features. Compared to the previously reported cationic variant $[Ir(L2)_2(bipy)]PF_6$, both neutral analogues display a bathochromically shifted ^{3}MLCT feature (Figures 5 and S3–S8).[7b]

Density Functional Theory (DFT). DFT calculations, performed on each complex discussed herein, support the assignments of the features in the absorption spectra through time-dependent DFT (TD-DFT). Qualitatively, the simulated absorption spectra (e.g., Figures 6 and S9–S17) are in reasonable agreement with the experimental absorption spectra, each with three main components in the same relative order of intensity as that of the absorption spectra, although the DFT procedure underestimates the absolute energy of all transitions (Table 4). The absorption bands of <450 nm are predominantly ^{1}MLCT in character because the occupied molecular orbitals involved in the excitation generally carry significant metal contributions (25–38%), while the unoccupied molecular orbitals are predominantly localized on the quinoxaline ligands. The calculations also predict that unoccupied molecular orbitals localized on either the picolinate or pyrazinoate ancillary ligands do not contribute

https://dx.doi.org/10.1021/acs.inorgchem.9b02991
Inorg. Chem. 2020, 59, 2266–2277

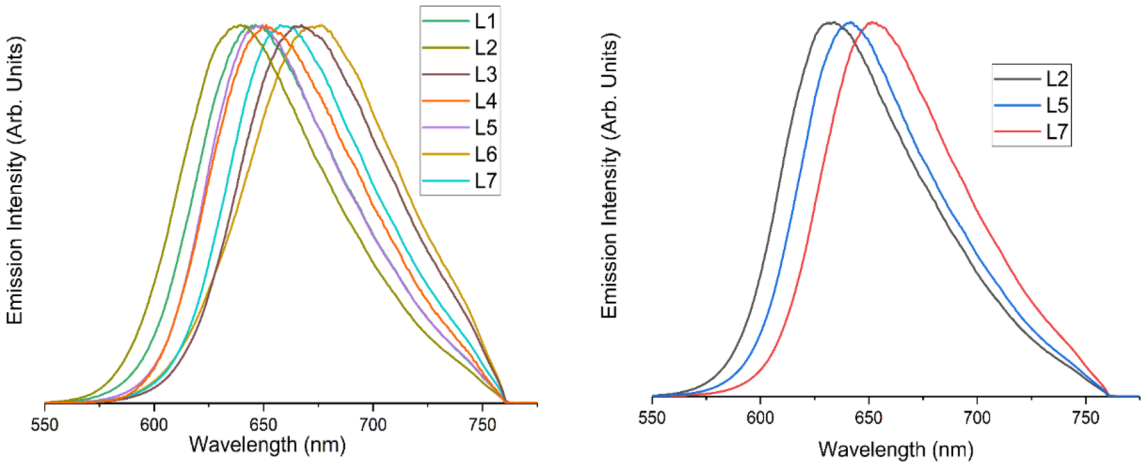

Figure 8. Emission spectra obtained for the picolinate complexes $[Ir(L)_2(pic)]$ (left) and the pyrazinoate complexes $[Ir(L)_2(pyz)]$ (right).

Table 8. Experimentally Determined Photophysical Properties of the Complexes[a]

complex	λ_{em} (nm)[b]	τ_{obs} (ns)[c]	ϕ (%)[d]	k_{nr} ($\times 10^6$)	k_r ($\times 10^5$)
$[Ir(L1)_2(pic)]$	647	303.9 ± 0.1	4.1	3.2	1.3
$[Ir(L2)_2(pic)]$	640	285.6 ± 0.5	6.8	3.3	2.4
$[Ir(L3)_2(pic)]$	665	266.3 ± 0.1	3.6	3.6	1.4
$[Ir(L4)_2(pic)]$	650	289 ± 0.1	4.8	3.3	1.7
$[Ir(L5)_2(pic)]$	648	306.0 ± 0.2	3.2	3.1	1.0
$[Ir(L6)_2(pic)]$	680	285.0 ± 0.5	2.7	3.4	0.9
$[Ir(L7)_2(pic)]$	653	290.4 ± 0.1	4.8	3.3	1.7
$[Ir(L2)_2(pyz)]$	633	351.0 ± 0.9	5.9	2.7	1.7
$[Ir(L5)_2(pyz)]$	641	328.2 ± 0.1	2.9	3.0	0.9
$[Ir(L7)_2(pyz)]$	651	352.0 ± 0.1	1.3	2.8	0.4

[a]Aerated chloroform solutions. [b]Emission wavelength; λ_{exc} = 355 nm. [c]Observed lifetime. [d]Quantum yield.

to the lowest unoccupied molecular orbital (LUMO) or LUMO+1 but rather dominate LUMO+2 (Tables 4 and 5). The simulated spectra all show a longest wavelength feature between 560 and 620 nm, which is predicted to be the spin-forbidden ^{3}MLCT (i.e., $S_0 \rightarrow T_1$) transition, which again corresponds to the low-intensity shoulder present in the experimentally obtained spectra of the complexes. Comprehensive details for each complex are presented in the Supporting Information.

Again, it is useful to compare these systems against their cationic complex analogues, $[Ir(L)_2(bipy)]PF_6$.[7b] In those systems, the complexes exhibited C_2 symmetry, and the two coordinated quinoxaline ligands were effectively degenerate, with equal contributions from each to the frontier orbitals, suggesting significant delocalization. Moving from a bipyridine ancillary ligand to the picolinate/pyrazinoate complexes reported herein removes this delocalization, breaking the symmetry of the system and splitting the orbital contributions of the quinoxalines.

The molecular orbitals within the picolinate complexes (Figures 7 and S18–S23) now form pseudodegenerate pairs with alternating contributions from each of the quinoxalines: e.g., the $[Ir(L1)_2(pic)]$ LUMO is made up of contributions of 36% and 59% (Table 6) from the quinoxalines Q1 and Q2, respectively, while the LUMO+1 shows the reverse (Q1 = 59%; Q2 = 36%). This effect is presumably due to differing interactions of the two quinoxalines with the asymmetric ancillary ligand. Notably, the pyrazinoate complexes do not show these pseudodegenerate pairs but, nonetheless, show a loss of degeneracy between the quinoxaline ligands, with greater contributions from one quinoxaline than the other. This effect likely contributes to the weak structure observed in the experimental absorption spectra of 300 nm < λ < 400 nm. The TD-DFT calculations also suggest that there are no singlet transitions (Table 6) at wavelengths long enough to account for the absorption at λ > 500 nm, whereas the lowest-energy singlet-to-triplet transition is within the 550 nm < λ < 620 nm region for all complexes. This is consistent with the observation of the long-wavelength, low-intensity absorption shoulder band observed in the experimental data (Figure 6). Figures S18–S26 and Tables S1–S9 contain the molecular orbital decomposition analyses for $[Ir(L)_2(pic)]$ (L = L2–L7) and $[Ir(L)_2(pyz)]$ (L = L2, L5, and L7).

Singlet and triplet geometries were calculated for each of the complexes along with stationary point-energy estimations of each spin state from the other geometry, allowing vertical transitions to be calculated. This was performed with the goal of simulating the spin-forbidden absorption and emission bands using approximations of the purely electronic component of the transition, without the geometric energy contributions associated with changing between the two different spin states. However, the calculated spin-forbidden absorption and emission bands significantly underestimate the energies involved; for example, the emission maximum for $[Ir(L2)_2(pic)]$ is experimentally observed at 640 nm (see the later discussion), yet the calculated $T_1 \rightarrow S_0$ vertical transition value was 689 nm. Therefore, this method can be considered as giving a good qualitative rather than quantitative insight into the effect that ligand structure alterations will have on the complex's spectral properties because the ordering of the complex emission centers is correct despite the energetic offset.

The predicted effects of quinoxaline ligand substitution were investigated by examining the energy values of the HOMO and LUMO for each of the complexes (Table 7). Electron-withdrawing groups are known to have a stabilizing effect on the metal-dominated HOMO through removal of the electron density, while electron-donating groups have the inverse effect.[24] Here, those complexes possessing quinoxaline ligands with electron-withdrawing groups (e.g., F, Cl) exhibit lower-energy values for the frontier orbitals. The LUMO is typically stabilized more effectively than the HOMO, a feature that can

https://dx.doi.org/10.1021/acs.inorgchem.9b02991
Inorg. Chem. 2020, 59, 2266–2277

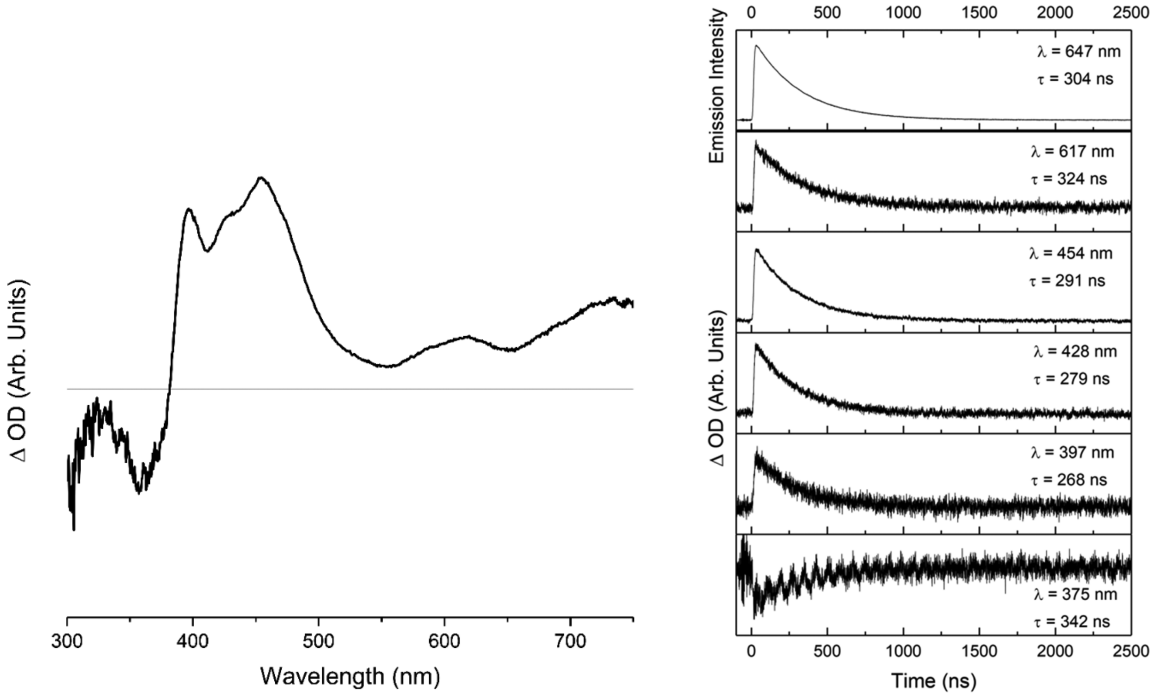

Figure 9. Left: Example of a TA spectrum using $[Ir(L1)_2(pic)]$. The gray horizontal line corresponds to a ΔOD value of zero, such that negative-trajectory features correspond to the depletion of a ground-state absorption and positive features correspond to excited-state absorption. Right: Kinetic traces of the major features of $[Ir(L1)_2(pic)]$. The top trace is an emission trace, and the bottom five are difference optical density measurements. All traces are fitted to monoexponential functions, and the obtained lifetimes are displayed alongside. Similar representations for all other complexes in the series are available in the Supporting Information.

be ascribed to the greater involvement of the quinoxaline ligands in the LUMO and thus a more pronounced effect as the electron affinity of the ligand is increased. This disparity between the effect on each orbital gives rise to slight differences in the emission and absorption energies observed for the complexes because the HOMO-to-LUMO gap is reduced for those with electron-withdrawing groups and increased for those with electron-donating groups (e.g., methyl), relative to the unsubstituted complex $[Ir(L1)_2(pic)]$. The phenyl-substituted complexes exhibit HOMO energy values very similar to those of their methylated counterparts but show lower LUMO values.

The effect of the ancillary ligand is somewhat similar: varying the ligand stabilizes or destabilizes the frontier orbitals of the complex by removing or increasing electron density on the metal center. In this case, both ligand types (picolinate and pyrazinoate) are relatively electron-withdrawing, and the effect is more pronounced for the pyrazinoates because of the presence of an additional N in the ring. Although electron withdrawal stabilizes the HOMO and LUMO, the relative stabilization is not identical with the effect of quinoxaline substitution. In this instance, the calculated energies of the molecular orbitals suggest that the pyrazinoate complexes have HOMO (0.1 eV) levels that are stabilized slightly more than the LUMO (~0.09 eV) compared to their picolinate counterparts. This effect gives rise to a predicted slight hypsochromic shift in the pyrazinoate complexes. The changes in the HOMO versus LUMO stabilization may be readily explained by the larger metal contribution to the HOMO. It is worth noting that the similarity in the band profile of the emission spectra regardless of the ancillary ligand, along with the almost identical nature of the long-wavelength ^{1}MLCT absorption bands displayed in Figure 5, illustrate that, although the ancillary ligand may tune the positions of the HOMO and LUMO orbitals, it does not significantly contribute to them or change their overall electronic character. This is consistent with the orbital decomposition analysis presented above.

Luminescence Properties of the Complexes. Emission spectra were obtained on each of the complexes using aerated chloroform and an excitation wavelength of 355 nm (Figure 8). Each of the neutral complexes was emissive in the red region of the spectrum between 633 and 680 nm, with quantum yields (ϕ) typically of ca. 5% (Table 8). All emission peaks appear as featureless broad bands. Observed emission lifetimes (τ_{obs}) were obtained from time-resolved data fitted to a mono-exponential function. The values for the rates of nonradiative (k_{nr}) and radiative (k_r) decays were calculated from the experimental data and show that $k_{nr} \gg k_r$ in all cases. The k_r values are indicative of a significant spin−orbit coupling (SOC) contribution but slightly lower than that reported for *fac*-$[Ir(ppy)_3]$, 4×10^5 s^{-1}.[25]

Compared to the corresponding cationic complexes $[Ir(L)_2(bipy)]PF_6$, the current series of compounds demonstrate bathochromically shifted emission maxima for a given quinoxaline ligand (Figure 8). As noted earlier, the trend across the series of complexes in the experimental emission maxima is quite well replicated using the computational methods discussed earlier. For example, $[Ir(L2)_2(pyz)]$, which was calculated to possess the largest HOMO−LUMO energy gap, also displayed the shortest-wavelength emission band. A comparison of the emission data for $[Ir(L2)_2(pic)]$ and $[Ir(L2)_2(pyz)]$ shows that the latter is indeed hypsochromically shifted. However, the cyclic voltammetry data showed that $[Ir(L2)_2(pyz)]$ possesses the smallest electrochemical band gap in the series of complexes. For a pure ^{3}MLCT

https://dx.doi.org/10.1021/acs.inorgchem.9b02991
Inorg. Chem. 2020, 59, 2266−2277

Table 9. Time-Resolved TA Properties of the Complexes

complex	ground-state bleach	excited-state absorption
$[Ir(L1)_2(pic)]^a$	375 nm (341.9 ± 7.9 ns)	397 nm (268.4 ± 3.0 ns)
		428 nm (279.3 ± 1.1 ns)
		454 nm (290.8 ± 0.5 ns)
		617 nm (324.2 ± 1.7 ns)
$[Ir(L2)_2(pic)]^a$	375 nm (332.3 ± 5.8 ns)	400 nm (304.6 ± 4.8 ns)
		410 nm (301.5 ± 2.0 ns)
		460 nm (320.9 ± 2.2 ns)
		600 nm (350.0 ± 2.0 ns)
$[Ir(L3)_2(pic)]^a$	368 nm (262.7 ± 3.8 ns)	410 nm (253.6 ± 0.7 ns)
	383 nm (245.7 ± 3.6 ns)	460 nm (274.1 ± 0.3 ns)
		649 nm(275.3 ± 2.3 ns)
$[Ir(L4)_2(pic)]^a$	375 nm (264.8 ± 7.3 ns)	402 nm (270.4 ± 0.9 ns)
		430 nm (260.2 ± 0.3 ns)
		450 nm (252.9 ± 0.3 ns)
		628 nm (304.6 ± 2.5 ns)
$[Ir(L5)_2(pic)]^a$	375 nm (324.7 ± 7.9 ns)	433 nm (326.3 ± 0.5 ns)
		455 nm (336.6 ± 0.9 ns)
		610 nm (328.9 ± 3.1 ns)
$[Ir(L6)_2(pic)]^a$	375 nm (292.4 ± 4.6 ns)	440 nm (297.5 ± 0.5 ns)
		470 nm (296.5 ± 0.4 ns)
$[Ir(L7)_2(pic)]^a$	375 nm (240.8 ± 4.0 ns)	430 nm (280.6 ± 0.4 ns)
		460 nm (268.1 ± 0.4 ns)
$[Ir(L2)_2(pyz)]^a$	372 nm (392.8 ± 15.2 ns)	419 nm (343.0 ± 3.9 ns)
		454 nm (382.2 ± 4.1 ns)
		585 nm (372.1 ± 2.9 ns)
$[Ir(L5)_2(pyz)]^a$	370 nm (328.8 ± 4.0 ns)	431 nm (349.1 ± 1.7 ns)
		459 nm (360.8 ± 1.3 ns)
		604 nm (380.0 ± 1.1 ns)
$[Ir(L7)_2(pyz)]^a$	355 nm (341.98 ± 4.6 ns)	440 nm (342.1 ± 0.8 ns)
		550 nm (395.2 ± 2.1 ns)
$[Ir(L2)_2(pic)]^b$	375 nm (1450 ± 24 ns)	400 nm (1345 ± 26 ns)
		410 nm (1284 ± 11 ns)
		460 nm (1285 ± 5 ns)
		600 nm (1267 ± 11 ns)
$[Ir(L2)_2(pyz)]^b$	372 nm (2159 ± 200 ns)	419 nm (1954 ± 40 ns)
		454 nm (1914 ± 33 ns)
		585 nm (1836 ± 34 ns)

[a]Aerated solutions in chloroform. [b]Deaerated solutions in chloroform.

emitter, a decrease in the electrochemical band gap would be expected to manifest in a bathochromic shift in λ_{em}.[26]

In the cases of $[Ir(L2)_2(pic)]$ and $[Ir(L2)_2(pyz)]$, additional deoxygenated luminescence lifetimes show modest increases to 1.283 and 1.883 μs, respectively. The magnitudes of these lifetimes are consistent with the reduction in $^3O_2$ collisional quenching, affording the definitive assignment that the emissive state is triplet in character. A comparison of the 77 K emission spectra (Figure S27) for $[Ir(L2)_2(pic)]$ and $[Ir(L2)_2(pyz)]$ (as 1:3 methanol/ethanol frozen glasses) shows emission profiles with a little vibronic definition and a slight hypsochromic shift to λ_{em} = 627 and 617 nm, respectively, which can be attributed to the rigidochromic effect of the frozen medium. Further, solvatochromic luminescence studies were conducted on $[Ir(L2)_2(pyz)]$ using a range of different solvents. The resultant data in toluene (λ_{em} = 622 nm), dichloromethane (626 nm), acetonitrile (632 nm), and dimethyl sulfoxide (636 nm) show a subtle bathochromic shift with increasing solvent polarity. Taken together, these observations suggest that some ^{3}MLCT character is likely to contribute to the emitting states of these complexes, as implied by the supporting DFT calculations.

Transient Absorption (TA) Spectra and Kinetics. TA spectra of the Ir(III) complexes showed three distinct features (Figures 9 and S28–S36). The first, ca. 350 < λ < 400 nm, is ascribed to a ground-state bleach: depletion of the ground-state ^{1}MLCT absorption band was seen in this region for all complexes. The second TA band is a strong positive-going feature in the 400 nm < λ < 500 nm region, with two peaks discernible in most of the spectra. These are assigned as triplet-to-triplet transitions because the lifetimes (Table 8) of the features correspond closely to those of the $T_1 \rightarrow S_0$ emission decay kinetics of the complexes (Figures 9 and S37–S45). Assignments of these features as photophysics arising from triplet-state manifolds were confirmed by extension of all observed transient lifetimes in the absence of O_2 (using $[Ir(L2)_2(pic)]$ and $[Ir(L2)_2(pyz)]$ as examples), consistent with rapid intersystem crossing occurring within the instrument response function (subnanosecond; Table 9).

TD-DFT calculations, performed at the triplet-state minimum-energy geometry, are also in agreement with this assignment, suggesting that there are a set of spin-allowed transitions within this wavelength region. Also visible in the TA

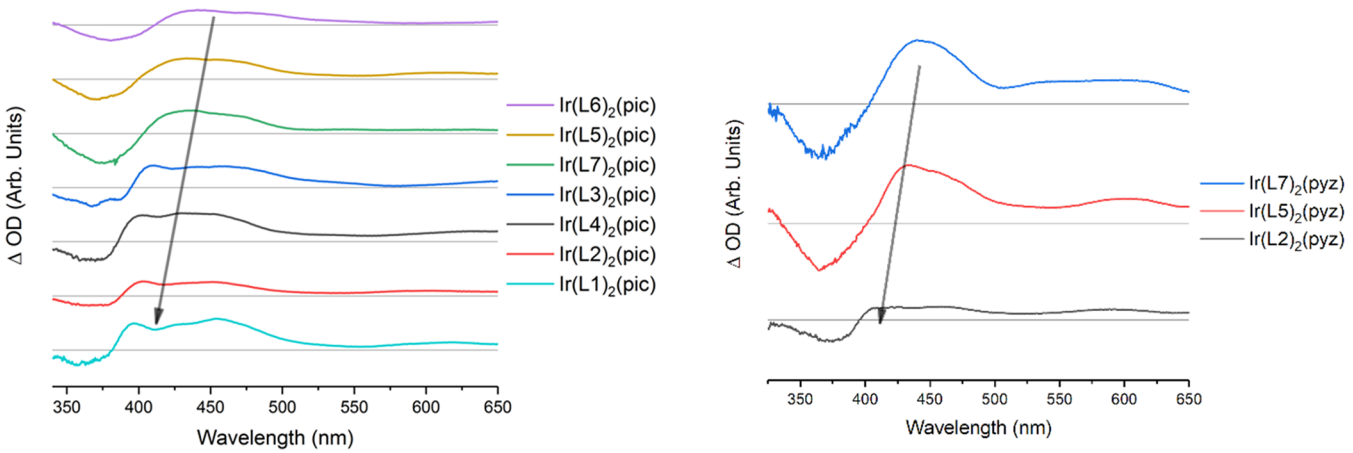

Figure 10. Comparison of the TA spectra of the picolinate (left) and pyrazinoate (right) Ir(III) complexes. The gray arrows highlight the spectral shifts described in the main text.

https://dx.doi.org/10.1021/acs.inorgchem.9b02991
Inorg. Chem. 2020, 59, 2266–2277

spectra is a broad, but weak, positive-going signal, centered at ca. λ = 600 nm. This was also assigned to a triplet-to-triplet absorption.

The structured absorption profiles in the region 400 nm < λ < 500 nm (notably in Figure 9) are ascribed to the pseudodegeneracy of the LUMO noted in the Density Functional Theory (DFT) section, resulting in numerous absorption features very close to each other in energy. This can be observed faintly in the ground-state absorption spectra of some of the complexes but is far more prominent in the TA spectra, highlighting the sensitivity of this technique as a means of characterization. Importantly, this structure to the absorption feature was not visible in the cationic variants $[Ir(L)_2(bipy)]PF_6$.[7b] As with the emission spectra, the TA spectra display a band shift (Figure 10) relative to $[Ir(L1)_2(pic)]$ depending on the ligand type. All of the picolinate complexes exhibit TA spectra that are bathochromically shifted relative to the $[Ir(L1)_2(pic)]$ complex. The magnitude of this shift depends on the quinoxaline ligand substitution, with phenyl-substituted ligands inducing a greater shift than simple halogenation at the quinoxaline ring (Table 9). It is noteworthy that very few examples of the TA spectra of organometallic complexes have been reported in the literature.[27]

CONCLUSIONS

In summary, this study has shown that heteroleptic neutral iridium(III) complexes, $[Ir(L)_2(N^O)]$ (where N^O = picolinate or pyrazinoate), incorporating cyclometalated quinoxaline ligands can demonstrate tunable emission in the long-wavelength part of the visible spectrum. The emission from these complexes likely arises from a mixture of quinoxaline-centered and ^{3}MLCT excited states. A combination of spectroscopic, electrochemical, and computational analyses lends support to the assignment and sheds light on the origin of the tunable nature of the emission. Crucially this insight shows that two strategies are available for modulating the emission energies of the complexes. First, substitution of the quinoxaline ligands influences both the HOMO and LUMO levels. Second, the ancillary picolinate or pyrazinoate ligands can modulate the HOMO level of the complex but are unlikely to contribute to any of the excited states that are relevant to the luminescence character. This final point is noteworthy because previous work[28] has suggested that the triplet excited-state level of related N^O ligands must be considered alongside any MLCT characteristics. Given the ease of functionalization of these complexes, our future studies will explore the application of these Ir(III) species in bioimaging studies, which can exploit the tuneability of long-wavelength luminescence properties.

ASSOCIATED CONTENT

Supporting Information

The Supporting Information is available free of charge at https://pubs.acs.org/doi/10.1021/acs.inorgchem.9b02991.

General information on synthetic methods, characterization, computational analyses, and photophysical studies and additional figures and tables (PDF)

Accession Codes

CCDC 1957545 contains the supplementary crystallographic data for this paper. These data can be obtained free of charge via www.ccdc.cam.ac.uk/data_request/cif, or by emailing data_request@ccdc.cam.ac.uk, or by contacting The Cambridge Crystallographic Data Centre, 12 Union Road, Cambridge CB2 1EZ, UK; fax: +44 1223 336033. Information on the data underpinning the results presented here, including how to access them, can be found in the Cardiff University data catalogue at http://doi.org/10.17035/d.2020.0098981053.

AUTHOR INFORMATION

Corresponding Authors

Joseph M. Beames − *School of Chemistry, Cardiff University, Cardiff CF10 3AT, Wales;* orcid.org/0000-0002-5508-8236; Email: beamesj@cardiff.ac.uk

Simon J. A. Pope − *School of Chemistry, Cardiff University, Cardiff CF10 3AT, Wales;* orcid.org/0000-0001-9110-9711; Email: popesj@cardiff.ac.uk

Authors

Thomas M. Stonelake − *School of Chemistry, Cardiff University, Cardiff CF10 3AT, Wales*

Kaitlin A. Phillips − *School of Chemistry, Cardiff University, Cardiff CF10 3AT, Wales*

Haleema Y. Otaif − *School of Chemistry, Cardiff University, Cardiff CF10 3AT, Wales*

Zachary C. Edwardson − *School of Chemistry, Cardiff University, Cardiff CF10 3AT, Wales*

Peter N. Horton − *U.K. National Crystallographic Service, Chemistry, Faculty of Natural and Environmental Sciences, University of Southampton, Highfield, Southampton SO17 1BJ, U.K.*

Simon J. Coles − *U.K. National Crystallographic Service, Chemistry, Faculty of Natural and Environmental Sciences, University of Southampton, Highfield, Southampton SO17 1BJ, U.K.;* orcid.org/0000-0001-8414-9272

Complete contact information is available at: https://pubs.acs.org/10.1021/acs.inorgchem.9b02991

Notes

The authors declare no competing financial interest.

ACKNOWLEDGMENTS

Cardiff University (Knowledge Economy Skills Scholarship to K.A.P.) and STG Aerospace are also thanked for financial support and technical input (Dr. Andrew Hallett and Dr. Sean O'Kell). We thank the Engineering and Physical Sciences Research Council (EPSRC) for funding the Ph.D. studentship of T.M.S. (Grant EP/L504749/1). We thank the staff of the EPSRC Mass Spectrometry National Service (Swansea University) and the EPSRC U.K. National Crystallographic Service at the University of Southampton.

REFERENCES

(1) *Iridium(III) in Optoelectronic and Photonics Applications*; Zysman-Colman, E., Ed.; John Wiley & Sons, Inc.: Chichester, West Sussex, U.K., 2017.

(2) (a) Lo, K.K-W.; Ng, D.C-M.; Chung, C.-K. First examples of luminescent cyclometalated iridium(III) complexes as labeling reagents for biological substrates. *Organometallics* **2001**, *20*, 4999−5001. (b) Zhao, Q.; Huang, C.; Li, F. Phosphorescent heavy-metal complexes for bioimaging. *Chem. Soc. Rev.* **2011**, *40*, 2508−2524. (c) Baggaley, E.; Gill, M. R.; Green, N. H.; Turton, D.; Sazanovich, I. V.; Botchway, S. W.; Smythe, C.; Haycock, J. W.; Weinstein, J. A.; Thomas, J. A. Dinuclear ruthenium(II) complexes as two-photon, time-resolved emission microscopy probes for cellular DNA. *Angew.*

Chem., Int. Ed. **2014**, *53*, 3367−3371. (d) Coogan, M. P.; Fernandez-Moreira, V. Progress with, and prospects for, metal complexes in cell imaging. *Chem. Commun.* **2014**, *50*, 384−399. (e) McKenzie, L. K.; Sazanovich, I. V.; Baggaley, E.; Bonneau, M.; Guerchais, V.; Williams, J. A. G.; Weinstein, J. A.; Bryant, H. E. Metal Complexes for two-photon photodynamic therapy: a cyclometallated iridium complex induces two-photon photosensitization of cancer cells under near-IR light. *Chem. - Eur. J.* **2017**, *23*, 234−238. (f) Baggaley, E.; Weinstein, J. A.; Williams, J. A. G. Time-Resolved Emission Imaging Microscopy Using Phosphorescent Metal Complexes: Taking FLIM and PLIM to New Lengths. *Struct. Bonding (Berlin, Ger.)* **2014**, *165*, 205−256. (g) Day, A. H.; Ubler, M. H.; Best, H. L.; Lloyd-Evans, E.; Mart, R. J.; Fallis, I. A.; Allemann, R. K.; Al-Wattar, E. A. H.; Keymer, N. I.; Buurma, N. J.; Pope, S. J. A. Targeted cell imaging properties of a deep red luminescent iridium(III) complex conjugated with a c-Myc signal peptide *Chem. Sci.* **2020** DOI: 10.1039/C9SC05568A.

(3) (a) Lamansky, S.; Djurovich, P.; Murphy, D.; Abdel-Razzaq, F.; Lee, H.-E.; Adachi, C.; Burrows, P. E.; Forrest, S. R.; Thompson, M. E. Highly Phosphorescent Bis-Cyclometalated Iridium Complexes: Synthesis, Photophysical Characterization, and Use in Organic Light Emitting Diodes. *J. Am. Chem. Soc.* **2001**, *123*, 4304−4312. (b) Ma, D.; Liu, R.; Zhang, C.; Qiu, Y.; Duan, L. High-efficiency organic light emitting diodes based on sublimable cationic iridium(III) complexes with sterically hindered spaces. *ACS Photonics* **2018**, *5*, 3428−3437. (c) Ma, D.; Zhang, C.; Liu, R.; Qiu, Y.; Duan, L. Controlling ion distribution for high performance organic light emitting diodes based on sublimable cationic iridium(III) complexes. *ACS Appl. Mater. Interfaces* **2018**, *10*, 29814−29823. (d) Tordera, D.; Pertegas, A.; Shavaleev, N. M.; Scopelliti, R.; Orti, E.; Bolink, H. J.; Baranoff, E.; Gratzel, M.; Nazeeruddin, M. K. Efficient orange light-emitting electrochemical cells. *J. Mater. Chem.* **2012**, *22*, 19264−19268. (e) Mills, I. N.; Porras, J. A.; Bernhard, S. Judicious design of cationic, cyclometalated Ir(III) complexes for photochemical energy conversion and optoelectronics. *Acc. Chem. Res.* **2018**, *51*, 352−364.

(4) (a) Prier, C. K.; Rankic, D. A.; MacMillan, D. W. C. Visible Light Photoredox Catalysis with Transition Metal Complexes: Applications in Organic Synthesis. *Chem. Rev.* **2013**, *113*, 5322−5363. (b) Zuo, Z.; Ahneman, D. T.; Chu, L.; Terrett, J. A.; Doyle, A. G.; MacMillan, D. W. C. Merging photoredox with nickel catalysis: Coupling of α-carboxyl sp^3-carbons with aryl halides. *Science* **2014**, *345*, 437−440. (c) Hallett, A. J.; White, N.; Wu, W.; Cui, X.; Horton, P. N.; Coles, S. J.; Zhao, J.; Pope, S. J. A. Enhanced photooxidation sensitizers: the first examples of cyclometalated pyrene complexes of iridium(III). *Chem. Commun.* **2012**, *48*, 10838−10840.

(5) Li, Y.; Dandu, N.; Liu, R.; Hu, L.; Kilina, S.; Sun, W. Nonlinear Absorbing Cationic Iridium(III) Complexes Bearing Benzothiazolyl-fluorene Motif on the Bipyridine (N∧N) Ligand: Synthesis, Photophysics and Reverse Saturable Absorption. *ACS Appl. Mater. Interfaces* **2013**, *5*, 6556−6570.

(6) (a) Sheet, S. J.; Sen, B.; Khatua, S. Organoiridium(III) complexes as luminescence color switching probes for selective detection of nerve agent simulation in solution and vapor phase. *Inorg. Chem.* **2019**, *58*, 3635−3645. (b) Law, W.H-T.; Leung, K.-K.; Lee, L.C-C.; Poon, C.-S.; Liu, H.-W.; Lo, K.K-W. Cyclometalated Iridium(III) Bipyridyl−Phenylenediamine Complexes with Multicolor Phosphorescence: Synthesis, Electrochemistry, Photophysics, and Intracellular Nitric Oxide Sensing. *ChemMedChem* **2014**, *9*, 1316−1329. (c) Lo, K.W-W.; Li, S.P-Y.; Zhang, K. Y. Development of luminescent iridium(III) polypyridine complexes as chemical and biological probes. *New J. Chem.* **2011**, *35*, 265−287.

(7) (a) Singh-Rachford, T. N.; Castellano, F. N. Photoupconversion based on sensitized triplet-triplet annihilation. *Coord. Chem. Rev.* **2010**, *254*, 2560−2573. (b) Phillips, K. A.; Stonelake, T. M.; Chen, K.; Hou, Y.; Zhao, J.; Coles, S. J.; Horton, P. N.; Keane, S. J.; Stokes, E. C.; Fallis, I. A.; Hallett, A. J.; O'Kell, S. P.; Beames, J. B.; Pope, S. J. A. Ligand-tuneable, red-emitting iridium(III) complexes for efficient triplet-triplet annihilation upconversion performance. *Chem. - Eur. J.* **2018**, *24*, 8577−8588. (c) Sun, J.; Wu, W.; Zhao, J. Long-Lived Room-Temperature Deep-Red-Emissive Intraligand Triplet Excited State of Naphthalimide in Cyclometalated Ir(III) Complexes and its Application in Triplet-Triplet Annihilation-Based Upconversion. *Chem. - Eur. J.* **2012**, *18*, 8100−8112.

(8) Henwood, A. F.; Zysman-Colman, E. Lessons learned in tuning the optoelectronic properties of phosphorescent iridium(III) complexes Chem. *Chem. Commun.* **2017**, *53*, 807−826.

(9) (a) Lai, P.-N.; Teets, T. S. Ancillary ligand effects on red-emitting cyclometalated iridium complexes. *Chem. - Eur. J.* **2019**, *25*, 6026−6037. (b) Lai, P.-N.; Brysacz; Alam, M. K.; Ayoub, N. A.; Gray, T. G.; Bao, J.; Teets, T. S. Highly efficient red-emitting bis-cyclometalated iridium complexes. *J. Am. Chem. Soc.* **2018**, *140*, 10198−10207.

(10) Ladouceur, S.; Zysman-Colman, E. A Comprehensive Survey of Cationic Iridium(III) Complexes Bearing Nontraditional Ligand Chelation Motifs. *Eur. J. Inorg. Chem.* **2013**, *2013*, 2985−3007.

(11) For example, see: Hierlinger, C.; Roisnel, T.; Cordes, D. B.; Slawin, A. M. Z.; Jacquemin, D.; Guerchais, V.; Zysman-Colman, E. An unprecedented family of luminescent iridium(III) complexes bearing a six-membered chelated tridentate C^N^C ligand. *Inorg. Chem.* **2017**, *56*, 5182−5188.

(12) Li, G. M.; Zhu, D. X.; Peng, T.; Liu, Y.; Wang, Y.; Bryce, M. R. Very High Efficiency Orange-Red Light-Emitting Devices with Low Roll-Off at High Luminance Based on an Ideal Host−Guest System Consisting of Two Novel Phosphorescent Iridium Complexes with Bipolar Transport. *Adv. Funct. Mater.* **2014**, *24*, 7420−7426.

(13) For example, see: Li, D.; Yan, X.; Hu, Y.; Liu, Y.; Guo, R.; Liao, M.; Shao, B.; Tang, Q.; Guo, X.; Chai, R.; Zhang, Q.; Tang, M. Two-photon image tracking of neural stem cells via iridium complexes encapsulated in polymeric nanospheres. *ACS Biomater. Sci. Eng.* **2019**, *5*, 1561−1568.

(14) Tsuboyama, A.; Iwawaki, H.; Furugori, M.; Mukaide, T.; Kamatani, J.; Igawa, S.; Moriyama, T.; Miura, S.; Takiguchi, T.; Okada, S.; Hoshino, M.; Ueno, K. Homoleptic Cyclometalated Iridium Complexes with Highly Efficient Red Phosphorescence and Application to Organic Light-Emitting Diode. *J. Am. Chem. Soc.* **2003**, *125*, 12971−12979.

(15) (a) Su, Y. J.; Huang, H. L.; Li, C. L.; Chien, C. H.; Tao, Y. T.; Chou, P. T.; Datta, S.; Liu, R. S. Highly Efficient Red Electrophosphorescent Devices Based on Iridium Isoquinoline Complexes: Remarkable External Quantum Efficiency Over a Wide Range of Current. *Adv. Mater.* **2003**, *15*, 884−888. (b) Li, C. L.; Su, Y. J.; Tao, Y. T.; Chou, P. T.; Chien, C. H.; Cheng, C. C.; Liu, R. S. Yellow and Red Electrophosphors Based on Linkage Isomers of Phenylisoquinolinyliridium Complexes: Distinct Differences in Photophysical and Electroluminescence Properties. *Adv. Funct. Mater.* **2005**, *15*, 387−395. (c) Huo, S.; Deaton, J. C.; Rajeswaran, M.; Lenhart, W. C. Highly Efficient, Selective, and General Method for the Preparation of Meridional Homo- and Heteroleptic Tris-cyclometalated Iridium Complexes. *Inorg. Chem.* **2006**, *45*, 3155−3157.

(16) Li, G.-N.; Dou, S.-B.; Zheng, T.; Chen, X.-Q.; Yang, X.-H.; Wang, S.; Sun, W.; Chen, G.-Y.; Mo, Z.-R.; Niu, Z.-G. Orange-Red Phosphorescent Iridium(III) Complexes Bearing Bisphosphine Ligands: Synthesis, Photophysical and Electrochemical Properties, and DFT Calculations. *Organometallics* **2018**, *37*, 78−86.

(17) (a) Guo, J.; Zhou, J.; Fu, G.; He, Y.; Li, W.; Lu, X. Two efficient near-infrared (NIR) luminescent [Ir(C^N)2(N^O)] characteristic complexes with 8-hydroxyquinoline (8-HQ) as the ancillary ligand. *Inorg. Chem. Commun.* **2019**, *101*, 69−73. (b) Li, C.-J.; Yin, S.-Y.; Wang, H.-P.; Wei, Z.-W.; Pan, M. Tuning Colorful luminescence of iridium(III) complexes from blue to near-infrared. *J. Photochem. Photobiol., A* **2019**, *379*, 99−104. (c) Phillips, K. A.; Stonelake, T. M.; Horton, P. N.; Coles, S. J.; Hallett, A. J.; O'Kell, S. P.; Beames, J. M.; Pope, S. J. A. Dual visible/NIR emission from organometallic iridium(III) complexes. *J. Organomet. Chem.* **2019**, *893*, 11−20. (d) Chen, H.-Y.; Yang, C.-H.; Chi, Y.; Cheng, Y.-M.; Yeh, Y.-S.; Chou, P.-T.; Hsieh, H.-Y.; Liu, C.-S.; Peng, S.-M.; Lee, G.-H. Room-temperature NIR phosphorescence of new iridium (III) complexes

https://dx.doi.org/10.1021/acs.inorgchem.9b02991
Inorg. Chem. 2020, 59, 2266−2277

with ligands derived from benzoquinoxaline. *Can. J. Chem.* **2006**, *84*, 309−318.
(18) (a) Routledge, J. D.; Hallett, A. J.; Platts, J. A.; Horton, P. N.; Coles, S. J.; Pope, S. J. A. Tuning the electronics of phosphorescent, amide-functionalised, cyclometalated Ir(III) complexes: syntheses, structures, spectroscopy and theoretical studies. *Eur. J. Inorg. Chem.* **2012**, *2012*, 4065−4075. (b) Smith, R. A.; Stokes, E. C.; Langdon-Jones, E. E.; Platts, J. A.; Kariuki, B. M.; Hallett, A. J.; Pope, S. J. A. Cyclometalated cinchophen ligands on iridium(III): towards water-soluble complexes with visible luminescence. *Dalton Trans.* **2013**, *42*, 10347−10357. (c) Jones, J. E.; Jenkins, R. L.; Hicks, R. S.; Hallett, A. J.; Pope, S. J. A. Water-soluble, luminescent iridium(III)-ytterbium-(III) complexes using dipyrido[3,2-a:2′,3′-c]phenazine derivatives as bridging units. *Dalton Trans.* **2012**, *41*, 10372−10381. (d) Lowe, J. A.; Stacey, O. J.; Horton, P. N.; Coles, S. J.; Pope, S. J. A. Alkyl chain functionalised cyclometalated platinum(II) complexes: syntheses, luminescence properties and X-ray crystal structure. *J. Organomet. Chem.* **2016**, *805*, 87−93. (e) Stacey, O. J.; Platts, J. A.; Coles, S. J.; Horton, P. N.; Pope, S. J. A. Phosphorescent, cyclometalated cincophen-derived platinum complexes: syntheses, structures, and electronic properties. *Inorg. Chem.* **2015**, *54*, 6528−6536. (f) Stacey, O. J.; Ward, B. D.; Coles, S. J.; Horton, P. N.; Pope, S. J. A. Chromophore-labelled, luminescent platinum complexes: syntheses, structures, and spectroscopic properties. *Dalton Trans.* **2016**, *45*, 10297−10307. (g) Stacey, O. J.; Amoroso, A.J.; Platts, J. A.; Horton, P. N.; Coles, S. J.; Lloyd, D.; Williams, C. F.; Hayes, A. J.; Dunsford, J. J.; Pope, S. J. A. Water soluble, cyclometalated Pt(II)-Ln(III) conjugates towards novel bimodal imaging agents. *Chem. Commun.* **2015**, *51*, 12305−12308.
(19) Langdon-Jones, E. E.; Hallett, A. J.; Routledge, J. D.; Crole, D. A.; Ward, B. D.; Platts, J. A.; Pope, S. J. A. Using substituted cyclometalated quinoxaline ligands to finely tune the luminescence properties of iridium(III) complexes. *Inorg. Chem.* **2013**, *52*, 448−456.
(20) (a) Schneidenbach, D.; Ammermann, S.; Debeaux, M.; Freund, A.; Zollner, M.; Daniliuc, C.; Jones, P. G.; Kowalsky, W.; Johannes, H.-H. Efficient and long-time stable red iridium(III) complexes for organic light emitting diodes based on quinoxaline ligands. *Inorg. Chem.* **2010**, *49*, 397−406. (b) Jing, Y.-M.; Wang, F.-Z.; Zheng, Y.-X.; Zuo, J.-L. Efficient deep red electroluminescence of iridium(III) complexes with 2,3-diphenylquinoxaline derivatives and tetraphenylimidodiphosphinate. *J. Mater. Chem. C* **2017**, *5*, 3714−3724. (c) Sun, W.; Pei, C.; Lu, T.; Cui, P.; Li, Z.; McCleese, C.; Fang, Y.; Kilina, S.; Song, Y.; Burda, C. Reverse saturable absorbing cationic iridium(III) complexes bearing the 2-(2-quinolinyl)quinoxaline ligand: effects of different cyclometalating ligands on linear and non-linear absorption. *J. Mater. Chem. C* **2016**, *4*, 5059−5072. (d) Tani, K.; Fujii, H.; Mao, L.; Sakurai, H.; Hirao, T. Iridium(III) complexes bearing quinoxaline ligands with efficient red luminescence properties. *Bull. Chem. Soc. Jpn.* **2007**, *80*, 783−788.
(21) Phillips, K. A. Development of luminescent iridium(III) and rhenium(I) complexes for optoelectronic applications. Ph.D. Dissertation, Cardiff University, Cardiff, U.K., 2019.
(22) Nonoyama, M. Benzo[*h*]quinolin-10-yl-N Iridium(III) Complexes. *Bull. Chem. Soc. Jpn.* **1974**, *47*, 767−768.
(23) Coles, S. J.; Gale, P. A. Changing and challenging times for service crystallography. *Chem. Sci.* **2012**, *3*, 683−689.
(24) (a) Lowry, M. S.; Bernhard, S. Synthetically tailored excited states: phosphorescent cyclometalated iridium(III) complexes and their applications. *Chem. - Eur. J.* **2006**, *12*, 7970−7977. (b) Adeloye, A. O.; Mphahlele, M. J.; Adekunle, A. S.; Rhyman, L.; Ramasami, P. Spectroscopic, Electrochemical and DFT Studies of Phosphorescent Homoleptic Cyclometalated Iridium(III) Complexes Based on Substituted 4-Fluorophenylvinyl- and 4-Methoxyphenylvinylquinolines. *Materials* **2017**, *10*, 1061−1082.
(25) Williams, J. A. G.; Wilkinson, A. J.; Whittle, V. L. Light-emitting iridium complexes with tridentate ligands. *Dalton Trans.* **2008**, 2081−2099.
(26) Flamigni, L.; Barbieri, A.; Sabatini, C.; Ventura, B.; Barigelletti, F. Photochemistry and Photophysics of coordination compounds: iridium. *Top. Curr. Chem.* **2007**, *281*, 143.
(27) Flamigni, L.; Ventura, B.; Barigelletti, F.; Baranoff, E.; Collin, J.-P.; Sauvage, J.-P. Luminescent Iridium(III)-Terpyridine Complexes − Interplay of Ligand Centred and Charge Transfer States. *Eur. J. Inorg. Chem.* **2005**, *2005*, 1312−1318.
(28) You, Y.; Park, S. Y. Inter-Ligand Energy Transfer and Related Emission Change in the Cyclometalated Heteroleptic Iridium Complex: Facile and Efficient Color Tuning over the Whole Visible Range by the Ancillary Ligand Structure. *J. Am. Chem. Soc.* **2005**, *127*, 12438−12439.

https://dx.doi.org/10.1021/acs.inorgchem.9b02991
Inorg. Chem. 2020, 59, 2266−2277